Int. J. Electrochem. Sci., 17 **(2022)** Article Number: 220456, doi: 10.20964/2022.04.03

International Journal of
ELECTROCHEMICAL
SCIENCE
www.electrochemsci.org

Effect of Fluid parameters on Erosion-corrosion behavior of Al-2%Zn coatings on AA5083 Aluminium Alloy in 3.5% NaCl

Yanming Xia[1], *Dejing Zhou*[2], *Zhiming Gao*[1,*], *Wenbin Hu*[1]

[1] Tianjin Key Laboratory of Composite and Functional Materials, School of Materials Science and Engineering, Tianjin University, Tianjin, 300354, China
[2] Yin Bang Clad Mat Co Ltd, Jiangsu Key Lab Clad Mat, Wuxi, 214145, China
[*]E-mail: gaozhiming@tju.edu.cn

Received: 19 December 2021 / *Accepted:* 1 February 2022 / *Published:* 4 March 2022

The erosion-corrosion behavior of Al-2%Zn coating in flowing 3.5% NaCl solution was investigated by using potentiodynamic polarization, electrochemical impedance spectroscopy and surface analysis techniques through a self-made impingement jet device. The results show that the corrosion process of the coating in a static solution is controlled by activation and mass transfer processes. In flowing solutions with or without sand, corrosion of the coating is an activation-controlled process. The flowing solution will accelerate the oxygen transfer process, resulting in a decrease in the cathodic Tafel slope and an increase in cathodic current density. Due to the rough surface of the coating, the direct impact of the fluid will destroy the corrosion product film, resulting in an increase in anodic current density. Sand particles mainly play a role in the erosion and destruction of the surface oxide film layer. Cu^{2+} ions and Hg^{2+} ions have a similar effect, as their concentration increases, the oxygen reduction reaction at cathode is weakened, so is the amount of oxide generated on the surface. Eventually, an increase in anodic current density and a negative shift in potential can be observed. Sand, Cu^{2+} ions and Hg^{2+} ions play a positive synergistic role in the erosion-corrosion process of the coating in the flowing 3.5% NaCl.

Keywords: Erosion-corrosion; Al-Zn coating; Cu^{2+}; Hg^{2+}; polarization curves

1. INTRODUCTION

Aluminum alloys are widely used in heat exchangers, radiators and transmission oil coolers because of their high specific strength, good thermal conductivity, corrosion resistance, and low density [1-3], and has replaced some of the conventional materials such as copper and stainless steel [4]. However, it is well known that aluminum alloys are highly susceptible to pitting corrosion [5-7] in seawater rich in aggressive chloride ions, and particles such as Fe^{3+} [8] and Cu^{2+} [9] can have a complex effect on the corrosion process of aluminum alloys. Joseph [10] et al. reported that aluminum was the anode in a wet/dry cycle corrosion test of copper/aluminum samples in natural seawater, and the

detection of very low levels of Cu^{2+} in the solution and the aluminum oxide film layer observed on the surface of the specimens were evidence that the corrosion of aluminum was significantly accelerated. Khedr [11] et al. found that Zn^{2+}, Hg^{2+} and Fe^{3+} are reduced to monomers on the surface of aluminum alloys in $C1^-$ containing solutions. The corrosion reaction is inhibited at low concentrations of metal cations due to the consumption of electrons by the reduction reaction, while at higher concentrations, the electric coupling formed between the metal and Al accelerates the corrosion of Al. In addition, aluminum alloys are relatively soft metals, so they can be susceptible to erosion-corrosion in fluid environments, resulting in shortened service life. Recent publications indicate a close relationship between the failure process of the material and the fluid condition [12,13]. Ramesh [14] et al. showed that pH is the parameter that has the greatest effect by comparing pH, impact velocity, and impact angle on the erosion-corrosion behavior of AA5083-AA6061 joints in the marine environment. Burstein [15] et al. described a positive synergy between erosion and corrosion of stainless steel in chloride solutions, which is greater at more inclined angles. It was found that there are many factors affecting erosion-corrosion and that due to their synergistic effect, the total weight loss of the material during E-C is much higher than that caused by pure corrosion or pure erosion alone [16-18].

The application of aluminum alloy is hindered due to the failure caused by the above reasons. Moreover, it is uneconomical and impractical to replace large components such as pipes frequently. Therefore, in order to solve the above problems, surface treatment techniques including electrodeposition [19], spraying [20] and organic coatings [21] have been applied and achieved significant results. Among these, aluminum-based composite coatings are widely used due to their excellent properties, which effectively slow down the process of material failure under a variety of conditions, such as corrosion [22,23], cavitation [24,25], and erosion-corrosion [26,27]. However, in the offshore flowing seawater, in addition to the previously mentioned flow velocity and sand particles, etc., which can affect the erosion-corrosion behavior of the coating, contaminants such as Cu^{2+} [28] and Hg^{2+} [8] are also present at the same time. The two ions mentioned above have a certain effect on the erosion-corrosion behavior of the coating which cannot be ignored. And to the best of our knowledge, there are no studies on the erosion-corrosion behavior of Al-Zn coatings in fluid sand-containing 3.5% NaCl solutions with Cu^{2+} and Hg^{2+}.

In this study, Al-2%Zn coating sprayed on AA5083 substrate, which is commonly used on the surface of open rack vaporizer (ORV) heat exchanger pipes, was studied. The erosion-corrosion behavior of the coating in a flowing NaCl solution containing Cu^{2+}, Hg^{2+} and sand particles was investigated by a self-made impingement jet system. Electrochemical tests including potentiodynamic polarization curves, corrosion potential and electrochemical impedance spectroscopy (EIS) and surface analysis methods including scanning electron microscopy (SEM), energy dispersive spectroscopy (EDS) were used to investigate the effect of Cu^{2+} and Hg^{2+} ions, sand on the erosion-corrosion of Al-2%Zn coatings.

2. EXPERIMENT

2.1. Material

AA5083 was used as the substrate in the current experiments with chemical composition of Mg (4.5), Mn (0.42), Si (0.16), Cu (0.18), Ti (0.15), Zn (0.25) and Al (Bal.). An Al-2%Zn coating was

prepared on the substrate using Al and Zn wires by flame spraying [29], and the morphology and chemical composition of the coating surface are shown in Fig. 1.

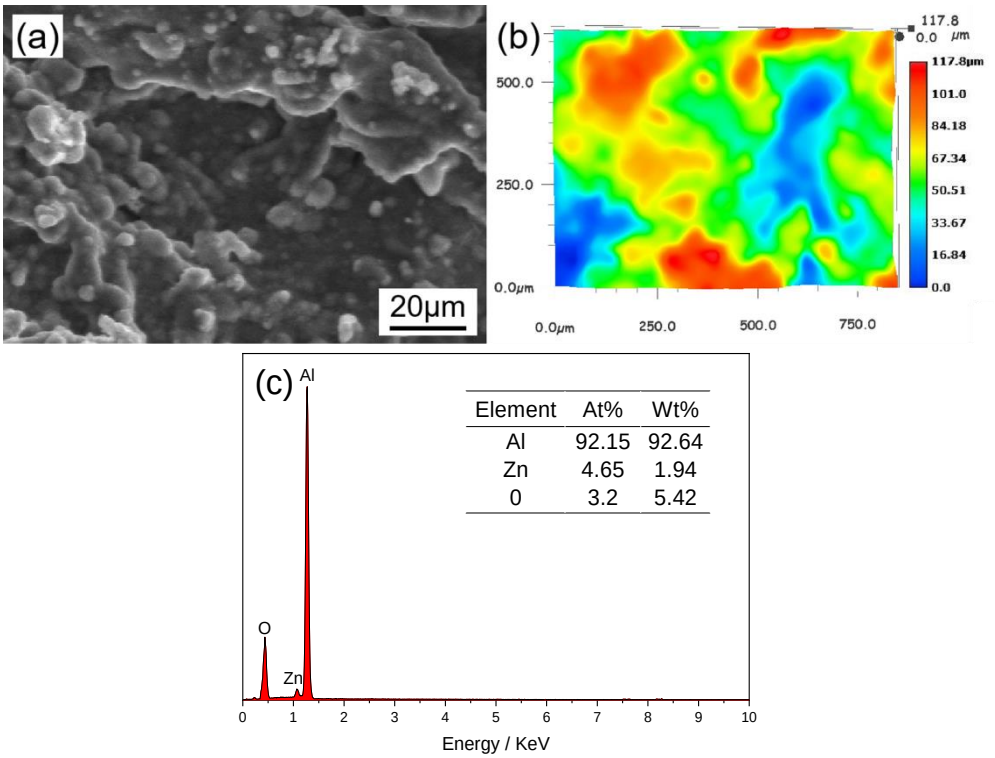

Figure 1. (a) Surface morphology, (b) 3D morphology and (c) EDS of the coating surface

2.2. Erosion–corrosion tests

Table 1. Fluid conditions in erosion-corrosion experiments

Sample No.	Fluid state
S0	Static 3.5% NaCl
S1	2 m/s 3.5% NaCl
S1-1	2 m/s 3.5% NaCl+300 mg/L sand
S1-2	2 m/s 3.5% NaCl+1 μg/L Cu^{2+}
S1-3	2 m/s 3.5% NaCl+10 μg/L Cu^{2+}
S1-4	2 m/s 3.5% NaCl+0.05 μg/L Hg^{2+}
S1-5	2 m/s 3.5% NaCl+0.3 μg/L Hg^{2+}
S2	2 m/s 3.5% NaCl+300 mg/L sand+1 μg/L Cu^{2+}+0.05 μg/L Hg^{2+}

The erosion-corrosion experiments of the coatings were performed using a self-made impingement jet device with a mechanism as described in [30]. For erosion-corrosion test, the specimens were cut into 15 × 15 mm working area, ultrasonically cleaned and placed in a desiccator.

Erosion-corrosion tests were conducted in 3.5% NaCl solution (pH 7.5) with different media added to simulate the coastal marine environment at an impact angle of 90° for 60 h, and the specific fluid states are shown in Table 1. Sand particles of size 500-600 μm were suspended in the medium. Scour corrosion tests were conducted. The specimens were placed at a distance of about 1 cm from the nozzle to ensure a stable flow rate. The surface of the worn specimen was observed using SEM (su1510). After the test, the corrosion products were removed and the weight loss rate was obtained by weighing the samples before and after the test with an electronic balance (0.0001g).

2.3. Electrochemical tests

The electrochemical tests of specimens during erosion-corrosion was conducted by using PARSTAT2273 electrochemical workstation with a three-electrode test cell, where saturated calomel electrode (SCE) is reference electrode, platinum sheet is counter electrode and the test samples are working electrodes. The potentiodynamic polarization curve was performed at 1mV/s. Electrochemical impedance spectroscopy was measured at stable potential with 10mV of perturbation, in the frequency range of 100 kHz to 10 mHz.

3. RESULTS

3.1. Electrochemical measurements

3.1.1. Effects of fluid flow and sand

Fig. 2 shows the polarization curves obtained for the samples in stationary and flowing (2 m/s) 3.5% NaCl solutions with and without sand, and the curves were fitted to obtain the corrosion potential (E_{corr}), the corrosion current density (I_{corr}), and the anodic (b_a) and cathodic tafel slopes (b_c),and the results are listed in Table 2. It can be seen that a passive region is observed under static conditions, which disappears under flow conditions. Under S1 conditions the corrosion potential shifts positively, accompanied by a decrease in the cathodic Tafel slope and an increase in the anodic current density. After adding sand to the solution, the corrosion potential shifted significantly negatively. In addition, the anodic current density increased significantly.

Fig. 3 shows the Nyquist and Bode diagrams of the samples at S0, S1 and S1-1 conditions. In the S1 solution, two capacitive semicircles can be observed at low and high frequencies. In the flowing solution with or without sand, the impedance spectrum changes significantly and the Nyquist plot contains a low-frequency inductive semicircle and a high-frequency capacitive semicircle. Moreover, the radius of the arc decreases significantly in the flowing sand-containing solution, meaning reduced corrosion resistance.

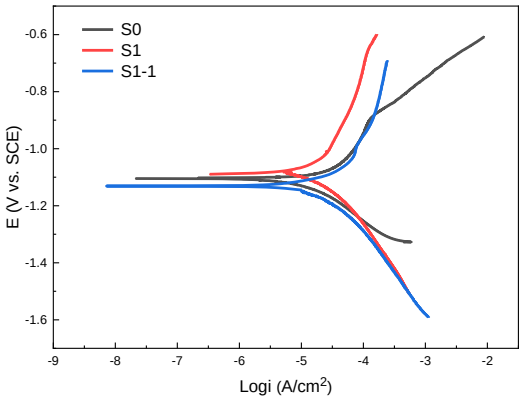

Figure 2. Polarization curves of samples under S0, S1 and S 1-1 conditions

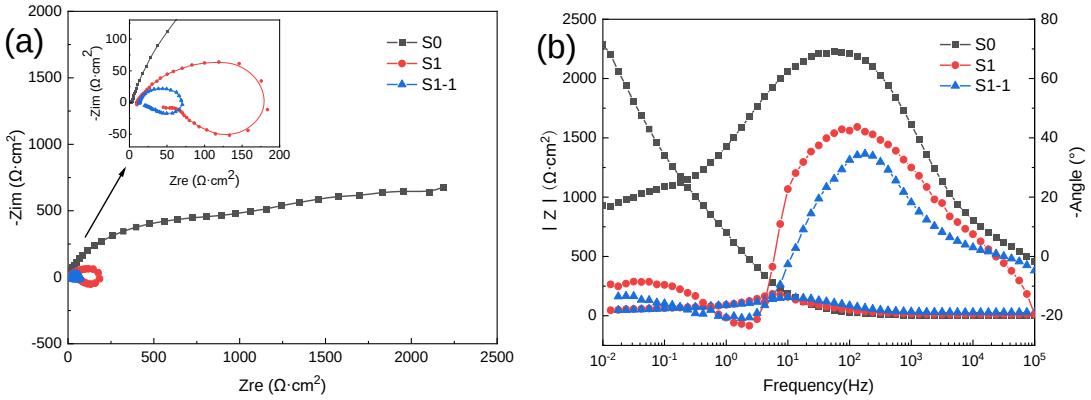

Figure 3. (a) Nyquist and (b) Bode plots of samples under S0, S1 and S 1-1 conditions

3.1.2. Effect of Cu^{2+} and Hg^{2+}

Fig. 4 shows the polarization curves of the samples in fluid solutions containing different types and concentrations of heavy metal ions. It can be seen that when heavy metal ions were added, active dissolution was observed in all conditions. When 1ug/L Cu^{2+} was added into the solution, no significant change in corrosion potential was observed, but the cathodic Tafel slope decreased significantly. The cathodic Tafel slope further decreased as the Cu^{2+} concentration increased to 10ug/L. Moreover, the corrosion potential shifts significantly negatively and the anodic current density increases. After Hg^{2+} ions were added to the solution, a similar phenomenon to that of Cu^{2+} ions was observed. With the increase of Hg^{2+} ion concentration from 0.05 to 0.3 ug/L, a negative shift of the potential, an increase of the anodic current density and a slight increase of the cathodic Tafel slope were observed.

Fig. 5 shows the Nyquist and Bode diagram for the samples under the above conditions. It can be seen that the impedance spectrum in all fluid conditions contain a low-frequency inductive semicircle and a high-frequency capacitive semicircle. The radius of the semicircle is the largest in the S1 condition and decreases with increasing ion concentration, both for Cu^{2+} and Hg^{2+} ions. In general, the decreasing size of semicircle implies a poorer corrosion resistance.

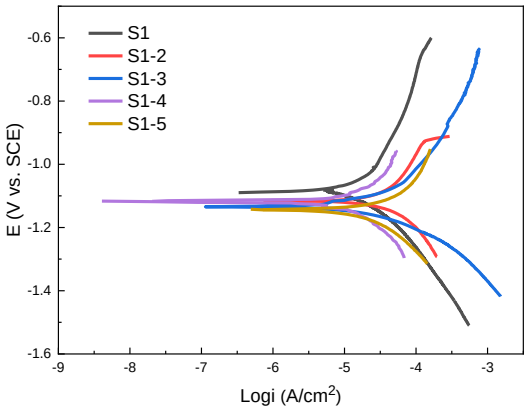

Figure 4. Polarization curves of samples under S1, S1-2, S1-3, S1-4 and S1-5 conditions

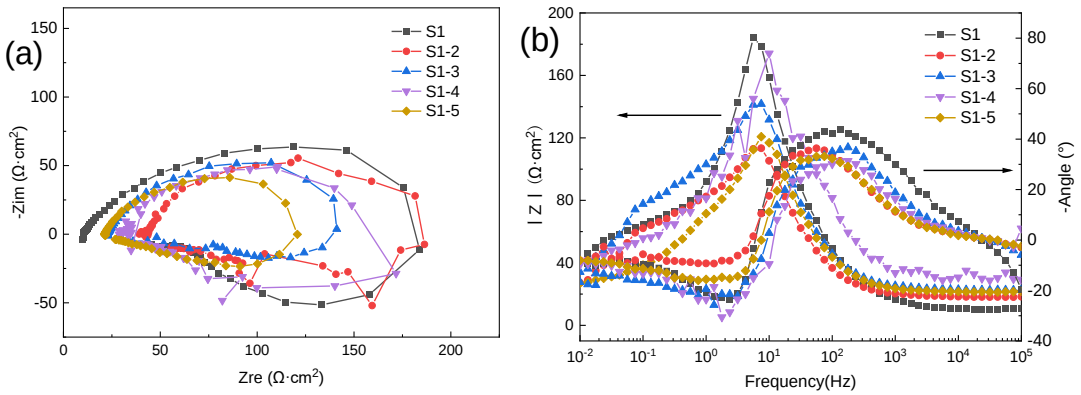

Figure 5. (a) Nyquist and (b) Bde plots of samples under S1, S1-2, S1-3, S1-4 and S1-5 conditions

3.1.3. Synergistic effect of various factors

Fig. 6 shows the polarization curves of the samples under the combined effect of flow rate (2 m/s), sand (300 ug/L), and heavy metal ions (1 ug/L Cu^{2+} and 0.05 ug/L Hg^{2+}). It can be seen that the corrosion potential is negatively shifted compared to the S1 condition and is lower than the values in all previous conditions. In addition to this, the cathodic Tafel slope decreases and the anodic current density increases significantly.

Fig. 7 shows the EIS of the samples at S1 and S2 conditions. It can be seen that the curves both consist of a capacitive semicircle and an inductive semicircle. And the radius of the semicircle reduces significantly under the coupled fluid conditions.

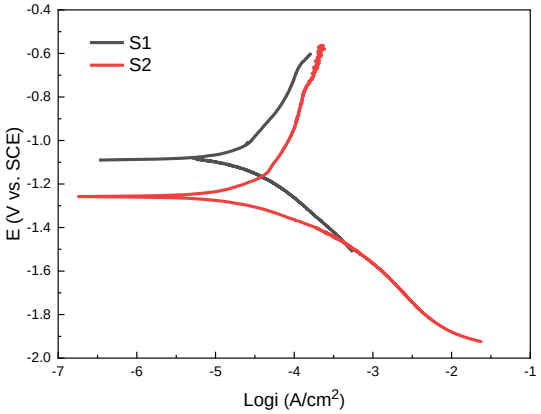

Figure 6. Polarization curves of samples under S1 and S2 conditions

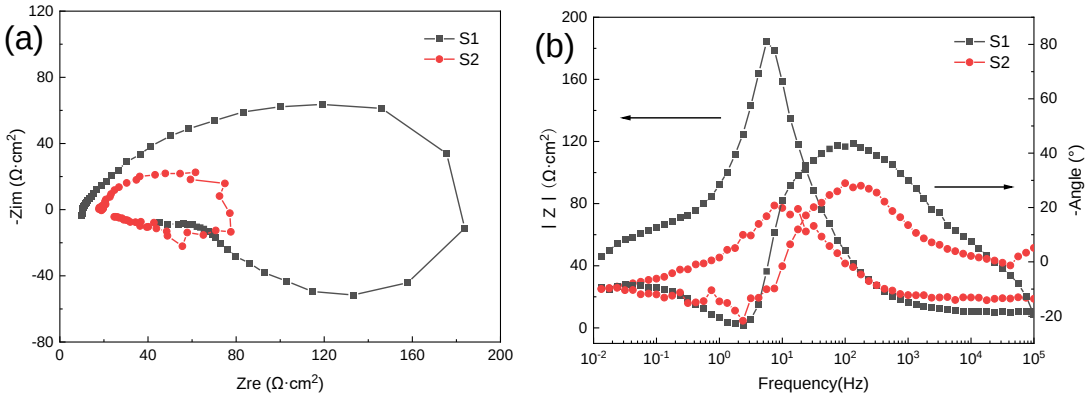

Figure 7. (a) Nyquist and (b) Bode plots of samples under S1 and S2 conditions

Table 2. Polarization parameters of the samples under different fluid conditions

Sample No.	E_{corr} / (V)	I_{corr} / (μA·cm^{-2})	b_a / (mV·dec^{-1})	b_c / (mV·dec^{-1})
S0	-1.105	11.48	463	161
S1	-1.090	27.09	352	301
S1-1	-1.131	58.16	245	315
S1-2	-1.120	35.01	326	287
S1-3	-1.134	41.62	292	254
S1-4	-1.116	29.72	338	295
S1-5	-1.143	52.47	315	286
S2	-1.261	62.20	242	278

3.2. Surface analysis and mass loss results

Fig. 8-Fig. 10 show the surface morphology of the samples under different conditions. Under the static condition, white granular corrosion products can be observed on the sample surface, and the coating surface is still intact. And in the flowing solution without sand, there are more corrosion products on the surface of the sample. However, under the effect of fluid, corrosion products are flaked and cracks appear on the surface. When sand is added to the fluid, only very little oxide remains on the sample surface, resulting in porous and broken surface. The morphology is similar in S1-2 and S1-4 conditions, with loose corrosion products covering the surface of the coating. As the concentration of both ions increases, the corrosion products become more porous, causing the exposure of the coating surface to solution. In the S2 condition only very little corrosion product remains on the coating surface and significant flaking occurs.

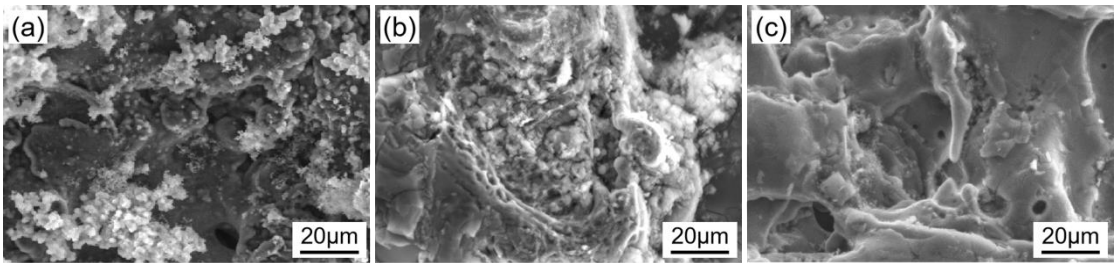

Figure 8. SEM of samples under (a) S0, (b) S1 and (c) S1-1 conditions

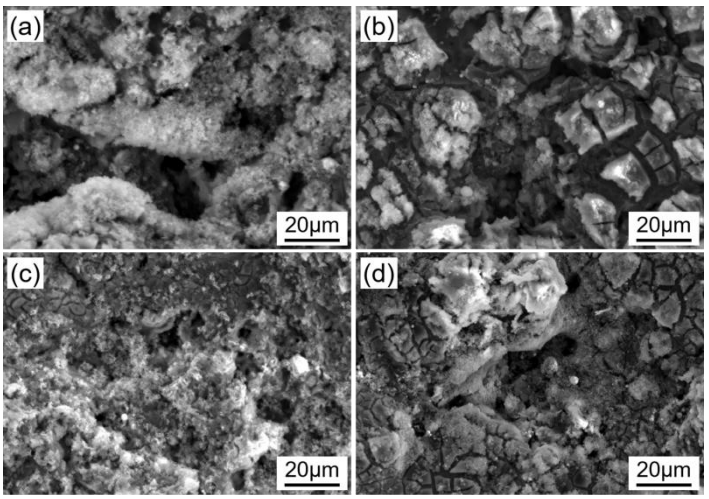

Figure 9. SEM of samples under (a) S1-2, (b) S1-3, (c) S1-4 and (d) S1-5 conditions

The results of EDS analysis of the samples after the erosion-corrosion experiment are shown in Fig. 11. The compositions of the sample surfaces in the solutions without heavy metal ions are all similar, taking Fig. 11a as an example, the main elements are Al, O, and Zn. The EDS results of the sample surface (the red box) under S2 conditions are shown in Fig. 11b. It can be seen that in addition to the above elements, small amounts of Cu and Si are present on the sample surface. This indicates that the

reduction reaction of Cu^{2+} ions occurs on the sample surface, and Si comes from the sand. Hg is not detected probably due to the extremely low content.

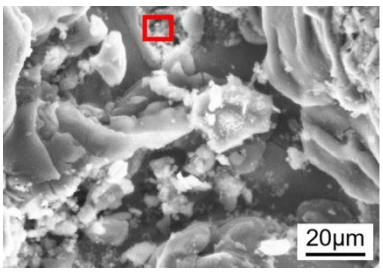

Figure 10. SEM of samples under S2

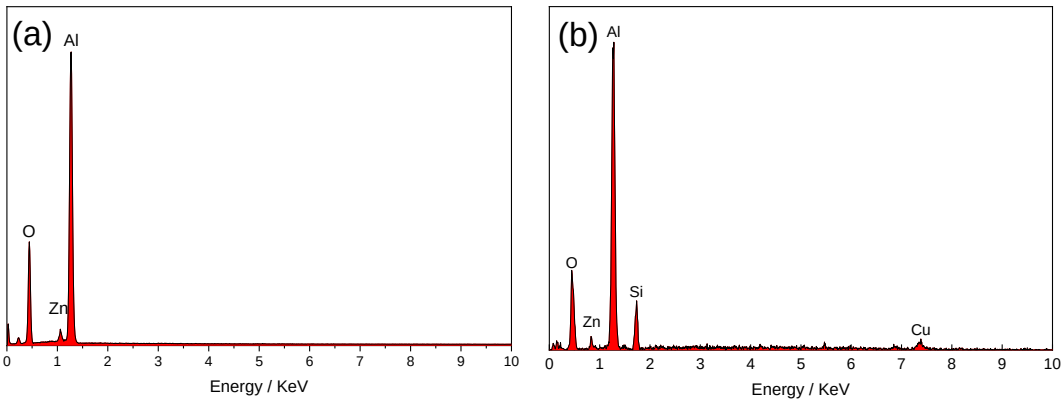

Figure 11. EDS results of samples surfaces under fluid conditions (a) without and (b) with Cu^{2+} and Hg^{2+}

From the data in Table 3, although the weight loss rate of specimens after 5 days of test is not obvious under different conditions, the effect of each factor on the loss rate of specimens can still be summarized. It can be seen that the loss rate of the specimens in the stagnant 3.5% NaCl solution is small, which increases slightly when the flow rate increases to 2 m/s. In this experiment, the increase of this value is due to that the coating surface is so rough that the corrosion products are not only subjected to normal stress but also shear stress, and finally cause the corrosion products film being destroyed and unstable. When sand is added to the solution, it can be seen that the loss rate of the specimen increases obviously, indicating that sand accelerates the peeling of the coating, which is caused by mechanical erosion. When Cu^{2+} and Hg^{2+} are added to the solution, the weight loss of the specimen does not change significantly probably due to the low content of heavy metal ions, which also indicates that electrochemical corrosion does not dominate the total material loss. Under S2 condition, the maximum rate is obtained, which is also mainly due to the increased normal and shear stresses caused by the addition of sand. From the above analysis, it can be concluded that mechanical erosion is the main cause of coating failure.

Table 3. Mass loss rate of the samples under different fluid conditions

Sample No.	S0	S1	S1-1	S1-2	S1-3	S1-4	S1-5	S2
Mass loss rate (mm/a)	0.0843	0.0958	0.1197	0.0966	0.0984	0.0958	0.0975	0.1437

4. DISCUSSION

The electrochemical reactions of Al-2%Zn coating in a static 3.5% NaCl solution are as follows:
Cathodic reaction:

$$O_2 + 2H_2O + 4e \rightarrow 4OH^- \quad (1)$$

Anodic reaction:

$$Al \rightarrow Al^{3+} + 3e \quad (2)$$

$$Zn \rightarrow Zn^{2+} + 2e \quad (3)$$

$$Al^{3+} + 3OH^- \rightarrow Al(OH)_3 \quad (4)$$

$$Zn^{3+} + 2OH^- \rightarrow Zn(OH)_2 \quad (5)$$

The cathodic reaction is reduction reaction of oxygen, the formed OH^- would combine with Al^{3+} to form oxide covering the surface of the specimen. The oxide will reduce the contact area between the coating surface and the solution, thus playing a role in preventing the corrosion.

In the stationary solution, the generation of oxide film enhances the stability of the coating surface. When the film is dense enough, the coating surface enters a stable passive state. And in the flowing solution, the oxygen diffusion is enhanced due to the liquid flow, causing the cathodic reaction enhanced, so is the cathodic Tafel slope and cathodic current density [31]. More OH^- combines with Al^{3+} to generate oxides covering the coating surface, therefore, the electrode potential shifts in the positive direction. However, because the coating itself is not smooth, the rough surface under the impact of the fluid is not only subjected to normal stresses, but also shear stresses. So that the corrosion products are partially destroyed and not dense, causing an increase in anodic current density, and therefore different from that described by Rajahram [32] et al. After the addition of sand to the solution, the oxide film is damaged by the impact of sand particles. Thus, the dissolution reaction of Al occurs on the surface of the coating, causing a decrease in potential. Also as mentioned before, the anodic current density increases. And sand has little effect on the cathodic reaction.

The EIS was analyzed for different fluid conditions to analyze the corrosion mechanism. In the stationary solution, two capacitive semicircles are observed and the R_p and R_t values are listed here in Table 3, where R_p is the modulus value at 0.01Hz, R_t is the maximum value of impedance. The oxygen content in the stationary solution becomes an controlled factor affecting the corrosion process. At this point the electrochemical reaction is controlled by both the mass transfer step and activation [33]. Under flow conditions, the mass transfer process of oxygen is significantly enhanced. The enhanced cathodic oxygen reduction reaction is expressed in the polarization curve as an increased cathodic Tafel slope. The more OH^- generated would combine with Al^{3+} on the surface of the specimen to form a denser

corrosion product film, which can effectively prevent the diffusion of the aggressive solution. This weakens the effective area of the anodic area and eventually leads to a decrease in anodic current density. At this point the corrosion process of the coating is controlled by activation. In fluids containing sand, the corrosion reaction is likewise an activation-controlled process. However, under the impact of sand particles, the oxide film is damaged and thinned. Thus, the active area on the electrode surface increases, which is manifested by an increase in anode current density and a negative shift in potential. Furthermore, in flow conditions with or without sand, inductive semicircles at low frequency can be observed. Generally, the inductive semicircles in erosion-corrosion process is associated with surface relaxation processes [34]. Under S1 and S1-2 conditions, the generation of a non-uniform film of corrosion products on the surface would increase the roughness of the electrode surface. In addition to this, adsorption of intermediate products of corrosion reactions on the electrode surface is also responsible for the appearance of the inductive semicircles. It can be seen that both solution flow and sand cause a significant decrease in the R_p and R_t, which also implies the non-dense film layer.

When Cu^{2+} and Hg^{2+} ions are added to the fluid, the following reactions also occur at the cathode site:

$$Cu^{2+} + 2e \rightarrow 2Cu \quad (6)$$

$$Hg^{2+} + 2e \rightarrow 2Hg \quad (7)$$

The above reaction will be gradually promoted with the increase of ion concentration, while the oxygen reduction reaction at the cathode is weakened, thus causing the cathode Tafel slope to decrease. Eventually, less OH^- is generated at the cathode resulting in a slower generation of corrosion product films. The increased anodic current density and negative potential shift indicate that the electrode surface is always in an activation-state. As shown in Table 3, the R_t decreases significantly with increasing heavy metal ion concentration relative to the value in fluid without ions. Therefore, heavy metal ions in the flowing environment can accelerate the corrosion rate of Al-2%Zn coating.

Table 3. The fitted R_{ct} of the samples under different fluid conditions

Sample No.	S0	S1	S1-1	S1-2	S1-3	S1-4	S1-5	S2
R_p ($\Omega \cdot cm^2$)	2291	55.81	46.66	34.11	29.01	40.47	26.99	25.68
R_t ($\Omega \cdot cm^2$)	—	184.1	146.8	141.7	113.4	164.1	120.7	80.76

Through the above analysis, under the coupling conditions of the factors, the oxide film on the coating surface is removed by the erosion effect of sand, and the percentage of cathodic oxygen is weakened due to the reduction reaction of heavy metal ions, so is the formation of oxides, and the coating is significantly activated. Therefore, each factor plays a positive synergistic effect on the erosion-corrosion of the coating.

5. CONCLUSION

1) Both activation and mass transfer processes in a stationary solution are control steps in the corrosion of Al-2%Zn coatings. Corrosion in a flowing solution with or without sand is the activation-controlled process.

2) The fluid promotes the cathode mainly by accelerating the mass transfer process, causing the cathodic Tafel slope to increase and the cathodic current density to decrease. The sand particles mainly make the anode current density increase by destroying the oxide film in the erosion process. In the flowing environment, Cu^{2+} ions and Hg^{2+} ions have similar effects. As their concentration increases, the oxygen reduction reaction is weakened and the amount of oxide generated on the coating surface decreases, which eventually causes the anodic current density to increase and the potential to shift negatively.

3) Sand, Cu^{2+} ions and Hg^{2+} ions in the fluid play a positive synergistic role in the erosion-corrosion process of the coating.

ACKNOWLEDGEMENTS
This work was supported by National Natural Science Foundation of China (No.51871164, No.51671144), Research on ORV Corrosion Mechanism and Application of Prevention and Control Technology (2019-XSKJ-04), Tianjin Science and Technology Project (No.20YDTPJC01780), and Shandong Taishan Industry Leading Talents Project (No.SF1503302301).

References

1. B. Wang, X.H. Chen, F.S. Pan, J.J. Mao and Y. Fang, *Trans. Nonferrous Met. Soc. China*, 25 (8) (2015) 2481.
2. J.Y. Jin and S.I. Hong, *Mater. Sci. Eng., A*, (1) (2014) 596.
3. C.Y. Meng, D. Zhang, C. Hua, L.Z. Zhang and J.S. Zhang, *J. Alloys Compd.*, 617 (25) (2014) 925.
4. W.S. Miller, L. Zhuang, J. Bottema, A.J. Wittebrood, P. De Smet, A. Haszler and A. Vieregge, *Mater. Sci. Eng., A*, 280 (2000) 37.
5. F. Yu and R. Akid, *Prog. Org. Coat.*, 102 (2017) 120.
6. K. Khanari and M. Finšgar, *Arabian J. Chem.*, 12 (8) (2019) 4646.
7. H. Allachi, F. Chaouket and K. Draoui, *J. Alloys Compd.*, 491 (1-2) (2010) 223.
8. O.K. Abiola and J. Otaigbe, *Corros. Sci.*, 50 (1) (2008) 242.
9. H.M. Obispo, L.E. Murr, R.M. Arrowood and E.A. Trillo, *J. Mate. Sci.*, 35 (14) (2000) 3479.
10. X. Joseph Raj and N. Rajendran, *J. Fail. Anal. Prev.*, 19 (2019) 250.
11. M.G.A. Khedr and A.M.S. Lashien, *J. Electrochem. Soc.*, 136 (4) (1989) 968.
12. M.Askari, M. Aliofkhazraei, S. Ghaffari and A. Hajizadeh, *J. Nat. Gas Sci. Eng.*, 58 (2018) 92.
13. J. Xia, Z. Li, J. Jiang, X. Wang and X. Zhang, *Int. J. Electrochem. Sci.,* 16 (2021) 1.
14. N.R. Ramesh and V.S. Senthil Kumar, *Appl. Ocean Res.*, 98 (2020) 102121.
15. G.T. Burstein and K. Sasaki, *Wear*, 240 (1-2) (2000) 80.
16. V.A.D. Souza and A. Neville, *Wear*, 263 (2007) 339.
17. B.W. Madsen, *Wear*, 123 (2) (1988) 127.
18. A. Neville, M. Reyes and H.Xu, *Tribol. Int.*, 35 (10) (2002) 643.
19. Y.W. Song, D.Y. Shan and E.H. Han, *Electrochim. Acta*, 53 (5) (2008) 2135.
20. E. Irissou, J.G. Legoux, B. Arsenault and C. Moreau, *J. Therm. Spray Technol.*, 16 (5) (2007) 661.

21. P. Huang, A. Somers, P.C. Howlett and M. Forsyth, *Surf. Coat. Technol.*, 303 (2016) 385.
22. C.T. Ye, L.N. Jia, G.X. Xu, F.F. Wang, X.C. Wang, X.C. Wang and H. Zhang, *Surf. Coat. Technol.*, 366 (2019) 214.
23. W. Liu, Q. Li and M.C. Li, *Corros. Sci.*, 121 (2017) 72.
24. Q.N. Song, Y. Tong, H.L. Li, H.N. Zhang, N.Xu, G.Y. Zhang, Y.F. Bao, W. Liu, Z.G. Liu and Y.X. Qiao, *J. Iron Steel Res. Int.*, (2021) 1.
25. D. Persson, D. Thierry and N. Lebozec, *Corros. Sci.*, 53 (2) (2011) 720.
26. D.K. Goyal, H. Singh, H. Kumar and V. Sahni, *Wear*, 289 (2012) 46.
27. J. Mehta, V.K. Mittal and P. Gupta, *J. Appl. Sci. Process Eng.*, 20 (4) (2017) 445.
28. I. Bakos and S. Szabó, *Corros. Sci.*, 50 (1) (2008) 200.
29. J. Huang, Y. Liu, J.H. Yuan and H. Li, *J. Therm. Spray Technol.*, 23 (4) (2014) 676.
30. M. Lavanya, Chin. *J. Chem. Eng.*, 28 (2) (2020) 340.
31. G.A. Zhang, L.Y. Xu and Y.F. Cheng, *Electrochim. Acta*, 53 (28) (2008) 8245.
32. S.S. Rajahram, T.J. Harvey and R. Wood, *Wear*, 267 (1-4) (2009) 244.
33. G.A. Zhang, L.Y. Xu and Y.F. Cheng, *Corros. Sci.*, 51 (2) (2009) 283.
34. L. Niu and Y.F. Cheng, *Wear*, 265 (3-4) (2008) 367.